Acta Crystallographica Section D
Biological Crystallography
ISSN 0907-4449

High-resolution structures of complexes of plant *S*-adenosyl-L-homocysteine hydrolase (*Lupinus luteus*)

Krzysztof Brzezinski,[a,b]* Zbigniew Dauter[b] and Mariusz Jaskolski[a,c]

[a]Center for Biocrystallographic Research, Institute of Bioorganic Chemistry, Polish Academy of Sciences, Poznan, Poland, [b]Synchrotron Radiation Research Section, MCL, National Cancer Institute, Argonne National Laboratory, Argonne, IL 60439, USA, and [c]Department of Crystallography, Faculty of Chemistry, A. Mickiewicz University, Poznan, Poland

Correspondence e-mail: kbrzezinski@anl.gov

Received 4 November 2011
Accepted 21 December 2011

PDB References: LlSAHase, complex with adenosine, 3ond; complex with adenine, 3one; complex with cordycepin, 3onf.

S-Adenosyl-L-homocysteine hydrolase (SAHase) catalyzes the reversible breakdown of *S*-adenosyl-L-homocysteine (SAH) to adenosine and homocysteine. SAH is formed in methylation reactions that utilize *S*-adenosyl-L-methionine (SAM) as a methyl donor. By removing the SAH byproduct, SAHase serves as a major regulator of SAM-dependent biological methylation reactions. Here, the first crystal structure of SAHase of plant origin, that from the legume yellow lupin (LlSAHase), is presented. Structures have been determined at high resolution for three complexes of the enzyme: those with a reaction byproduct/substrate (adenosine), with its non-oxidizable analog (cordycepin) and with a product of inhibitor cleavage (adenine). In all three cases the enzyme has a closed conformation. A sodium cation is found near the active site, coordinated by residues from a conserved loop that hinges domain movement upon reactant binding. An insertion segment that is present in all plant SAHases is located near a substrate-pocket access channel and participates in its formation. In contrast to mammalian and bacterial SAHases, the channel is open when adenosine or cordycepin is bound and is closed in the adenine complex. In contrast to SAHases from other organisms, which are active as tetramers, the plant enzyme functions as a homodimer in solution.

1. Introduction

S-Adenosyl-L-methionine (SAM) is the most common methyl-group donor in the cellular methylation (Richards *et al.*, 1978) of a wide range of substrates from small-molecule compounds, such as norepinephrine, catecholamines and phospholipids, to macromolecules, including proteins, nucleic acids and polysaccharides. Biogenesis of the ribosome also involves nucleotide methylations (van Buul *et al.*, 1983; Lafontaine *et al.*, 1994; Housen *et al.*, 1997; Ofengand, 2002; Seidel-Rogol *et al.*, 2003). At the epigenetic level, gene expression is regulated by the methylation of genomic DNA and histones (Kinoshita *et al.*, 2004; Mull *et al.*, 2006). Methylation has been linked to suppression of gene expression and to transcriptional or post-trancriptional gene silencing (Elmayan *et al.*, 1998; Morel *et al.*, 2000; Jones *et al.*, 2001; Rocha *et al.*, 2005). During methyl-group transfer, a byproduct, *S*-adenosyl-L-homocysteine (SAH), is formed which is a strong inhibitor of SAM-dependent methyltransferases. Two enzymes are involved in the removal of SAH. 5′-Methylthioadenosine/*S*-adenosyl-L-homocysteine (MTA/SAH) nucleosidase (EC 3.2.2.9) metabolizes SAH to adenine and *S*-ribosyl-L-homocysteine. This enzyme is mainly active in pathogenic or endosymbiotic organisms (which lack an SAHase gene), the lifestyle of which results in a reduction in the number of genes and the size of

the genome (Stępkowski *et al.*, 2005). The second enzyme, *S*-adenosyl-L-homocysteine hydrolase (SAHase; EC 3.3.1.1), catalyzes the reversible breakdown of *S*-adenosyl-L-homocysteine to adenosine (Ado) and homocysteine (Hcy) (de la Haba & Cantoni, 1959). By removing SAH, *S*-adenosyl-L-homocysteine hydrolase serves as an important regulator of SAM-dependent methylation reactions. The enzyme controls the SAM:SAH ratio, which is perceived to be an indicator of the transmethylation activity of the cell (Poulton & Butt, 1975; Chiang & Cantoni, 1979; Chiang, 1998). The equilibrium of the reaction catalyzed by SAHase is shifted far towards the direction of SAH synthesis. In addition, SAHase activity is inhibited by adenosine, which is a product of the hydrolysis reaction (de la Haba & Cantoni, 1959; Poulton & Butt, 1976). Under physiological conditions, the removal of Ado and Hcy is rapid and the net result is SAH hydrolysis (Richards *et al.*, 1978). In mammalian cells adenosine is metabolized to inosine by adenosine deaminase (ADA; EC 3.5.4.4; Migchielsen *et al.*, 1995), whereas in plants adenosine kinase (ADK; EC 2.7.1.20) is involved in the removal of adenosine (Moffatt *et al.*, 2002). Homocysteine is used for the regeneration of methionine and for the synthesis of cysteine.

Transmethylation reactions and their coupled regulation processes are crucial for growth and development in plants. Over one-third of the total DNA in *Arabidopsis thaliana* is methylated (Zhang *et al.*, 2006). Chlorophyll biosynthesis also involves a SAM-dependent transmethylation step (Alawady & Grimm, 2005). In plant metabolism, SAM is not only a methyl-group donor. After decarboxylation, it is a propylamine-group donor in polyamine biosynthesis. It is also a precursor in the biosynthesis of ethylene, a phytohormone that induces fruit maturation. Any perturbation of the SAM:SAH ratio may affect not only transmethylation reactions but also other processes involving SAM. Therefore, the concentrations of SAM and SAH must be strictly controlled, especially during critical developmental periods, and plants seem to be particularly sensitive to accurate SAM:SAH ratios (Fulneček *et al.*, 2011). In tobacco, for instance, the inhibition of SAHase in seeds resulted in mitotic transmission of hypomethylated DNA to adult plants, in pleiotropic developmental defects and in deregulation of floral genes (Fulneček *et al.*, 2011). In *A. thaliana*, cytokinin hormones up-regulate the methylation potential and promote DNA methylation. Li *et al.* (2008) have shown that the cytokinins increase the expression of DNA methyltransferases. Furthermore, the expression of *S*-adenosyl-L-homocysteine hydrolase and adenosine kinase is induced. On the other hand, a reduced methylation potential leads to cytokinin synthesis and expression of genes from the methylation pathway. By the induction of many genes that are responsible for methylation processes and also for their regulation, cytokinins precisely control the transmethylation cycle (Pereira *et al.*, 2007; Li *et al.*, 2008).

SAHases are oligomeric enzymes that are typically active as homotetramers. Plant SAHases are an exception in this respect as they have been reported to function as homodimers (Guranowski & Pawełkiewicz, 1977; Brzezinski *et al.*, 2008). An SAHase protomer has a distinct two-domain fold, with a deep crevice separating the N- and C-terminal domains. All *S*-adenosyl-L-homocysteine hydrolases require a tightly but noncovalently bound NAD^+ cofactor for their activity, which must be present in each subunit. All archaeal and some bacterial SAHase sequences are shorter (with a total length of about 420–430 residues) than those from most eukaryotes and bacteria (470–495 residues). The differences in polypeptide length reflect a lack of eight amino-acid residues at the C-terminal tail of archaeal-type SAHases and the presence of an insert of about 40 amino-acid residues in most bacterial sequences. This additional segment is also present in all plant SAHases and in some other eukaryotic enzymes, but is absent from fungal, insect and vertebrate enzymes (Stępkowski *et al.*, 2005). Structural knowledge of SAHases is mainly based on crystallographic studies of eukaryotic and prokaryotic enzymes from *Homo sapiens* (Turner *et al.*, 1998; Yang *et al.*, 2003), *Rattus norvegicus* (Hu *et al.*, 1999; Huang *et al.*, 2002), *Plasmodium falciparum* (Tanaka *et al.*, 2004), *Trypanosoma brucei* (PDB entry 3h9u; Structural Genomics Consortium, unpublished work), *Leishmania major* (PDB entry 3g1u; Structural Genomics Consortium, unpublished work), *Mycobacterium tuberculosis* (Reddy *et al.*, 2008), *Burkholderia pseudomallei* (PDB entry 3glq; Seattle Structural Genomics Center for Infectious Disease, unpublished work) and *Brucella melitensis* (PDB entry 3n58; Seattle Structural Genomics Center for Infectious Disease, unpublished work). The structures illustrate that SAHases undergo a significant conformational transformation upon substrate binding. A comparison of the conformation of the enzyme in the open form (rat SAHase complexed with NAD^+) with that in the closed form (SAHases complexed with NAD^+ and Ado or its analogs) reveals that the crevice between the two domains of a subunit is closed upon substrate binding.

In the present study, we determined high-resolution crystal structures of a recombinant plant *S*-adenosyl-L-homocysteine hydrolase corresponding to the sequence encoded by the *Lupinus luteus shh-1* gene (LlSAHase; Brzeziński *et al.*, 2001) crystallized as complexes with adenosine and cordycepin (3′-deoxyadenosine), which were added to the crystallization buffer. Cocrystallization with 2′-deoxyadenosine resulted in cleavage of the ligand molecule. In the crystallized complex, only the purine molecule occupies the binding site. The homodimeric state of this plant SAHase in solution has been confirmed by two experimental methods: ultracentrifugation and size-exclusion chromatography. Enzymatic assays were carried out to evaluate the kinetic parameters of recombinant LlSAHase and to establish the inhibitory potential of selected ligands.

2. Materials and methods

2.1. Crystallization and data collection

The purification of LlSAHase and the crystallization of its complexes was carried out as described in Brzezinski *et al.* (2008). Briefly, protein solution (2.0 mg ml^{-1} measured spectrophotometrically at 280 nm) was incubated overnight with

Table 1
Crystallographic data and refinement statistics.

Values in parentheses are for the last resolution shell.

Data set	LlSAHase–adenosine	LlSAHase–adenine	LlSAHase–cordycepin
Data-collection and processing statistics			
Beamline	EMBL/DESY X13	EMBL/DESY X13	EMBL/DESY X12
Wavelength (Å)	0.8086	0.8086	1.0000
Temperature (K)	100		
Space group	$P4_32_12$		
Unit-cell parameters (Å)			
a	122.4	122.0	122.6
c	126.6	126.4	126.6
Mosaicity (°)	0.38	0.53	0.50
Resolution range (Å)	20.0–1.17 (1.19–1.17)	20.0–1.35 (1.37–1.35)	50.0–2.00 (2.07–2.00)
Total reflections	3420366	1855699	691022
Unique reflections	319469	206827	65547
Completeness (%)	99.9 (98.5)	99.3 (98.2)	99.7 (100)
Multiplicity	10.7 (5.3)	9.0 (6.2)	10.5 (9.5)
$\langle I/\sigma(I)\rangle$	38.3 (2.3)	28.1 (2.2)	17.5 (3.1)
$R_{\rm merge}$†	0.057 (0.708)	0.070 (0.670)	0.131 (0.686)
Refinement statistics			
Resolution (Å)	20.0–1.17	20.0–1.35	50.0–2.00
Working/test reflections‡	315006/1093	204245/1057	64344/1119
$R/R_{\rm free}$§	0.128/0.159	0.128/0.163	0.156/0.201
Protein/water atoms	7516/1439	7516/1225	7500/637
No. of ions (sodium/Tris)	2/3	2/3	2/1
R.m.s.d. from ideality			
Bond lengths (Å)	0.019	0.018	0.015
Bond angles (°)	1.93	1.74	1.48
Average *B* factor (Å^2)	11.9	13.8	18.7
Ramachandran statistics (%)			
Most favored regions	91.4	92.0	90.7
Allowed regions	8.6	8.0	9.3
PDB code	3ond	3one	3onf

† $R_{\rm merge} = \sum_{hkl}\sum_i |I_i(hkl) - \langle I(hkl)\rangle|/\sum_{hkl}\sum_i I_i(hkl)$, where $\langle I(hkl)\rangle$ is the average intensity of reflection *hkl*. ‡ Negative intensities were excluded from refinement. § $R = \sum_{hkl}||F_{\rm obs}| - |F_{\rm calc}||/\sum_{hkl}|F_{\rm obs}|$, where $F_{\rm o}$ and $F_{\rm c}$ are the observed and calculated structure factors, respectively. $R_{\rm free}$ is calculated analogously for the test reflections, which were randomly selected and excluded from the refinement.

2 m*M* adenosine (crystal *A*), 2′-deoxyadenosine (crystal *B*) or cordycepin (crystal *C*) at 277 K. Crystals were obtained using 20%(*w*/*v*) PEG 4000, 10%(*v*/*v*) 2-propanol, 0.1 *M* Tris–HCl pH 8.0. X-ray diffraction data were measured on EMBL beamline X13 (crystals *A* and *B*) or beamline X12 (crystal *C*) of the DESY synchrotron (Hamburg, Germany) to resolutions of 1.17, 1.35 and 2.00 Å, respectively. All crystals were tetragonal and isomorphous. They belonged to space group $P4_32_12$. All diffraction images were processed and scaled with *HKL*-2000 (Otwinowski & Minor, 1997). Data-collection and processing statistics are shown in Table 1.

2.2. Structure determination and refinement

2.2.1. LlSAHase–adenosine complex. The structure was solved as described previously (Brzezinski *et al.*, 2008) by molecular replacement using the program *Phaser* (McCoy *et al.*, 2007). Chain *A* of *P. falciparum* SAHase (PDB entry 1v8b; Tanaka *et al.*, 2004) was used as the search model. The correct solution was found in space group $P4_32_12$ for two protomers in the asymmetric unit, which create a dimer corresponding to the active form of this plant enzyme. Anisotropic stereochemically restrained structure-factor refinement was carried out in *REFMAC*5 (Murshudov *et al.*, 2011) using maximum-likelihood targets. The electron density of the final model, which included two molecules of adenosine, two molecules of NAD^+ and 1439 water molecules, was of superb quality and only one N-terminal glycine residue (a cloning artifact) of chain *A* was not included in the final set of coordinates. Additionally, two Na^+ and three Tris ions were identified in the asymmetric unit. The identity of the metal cations was confirmed using the calcium bond-valence sum (CBVS) method (Müller *et al.*, 2003).

2.2.2. LlSAHase–adenine complex. The above model of the LlSAHase–adenosine complex stripped of all water molecules, ions and ligands was placed into the nearly identical unit cell of the LlSAHase–adenine crystal. A difference Fourier map showed that the active site only contained an adenine molecule, which is a product of 2′-deoxyadenosine hydrolysis (Abeles *et al.*, 1980, 1982). Anisotropic stereochemically restrained structure-factor refinement was carried out in *REFMAC*5 (Murshudov *et al.*, 2011) using maximum-likelihood targets. The electron density was very well defined for all of the protein residues except for the N-terminal Gly residue of chain *A*. Each subunit binds small-molecule ligands as in the LlSAHase–adenosine complex, except that adenine replaces adenosine. Na^+ and Tris ions were present as in the above structure. 1225 water molecules were identified in the asymmetric unit of this crystal.

2.2.3. LlSAHase–cordycepin complex. The LlSAHase–adenosine complex model stripped of all water molecules, ions and ligands was placed into the nearly identical unit cell of the LlSAHase–cordycepin crystal. Isotropic stereochemically restrained structure-factor refinement was carried out in *REFMAC*5 (Murshudov *et al.*, 2011), with the inclusion of three TLS groups (Winn *et al.*, 2001) per protein chain. The three N-terminal residues of chain *A* (GSH–, a cloning artifact) were not included in the final model. Each protomer binds one cordycepin molecule in the active site. There are two Na^+ ions and one Tris molecule as in the above crystal structures. 637 water molecules were identified in the asymmetric unit of this crystal.

2.2.4. Final refinements and model statistics. Rounds of *REFMAC*5 refinement were interspersed with manual model rebuilding in *Coot* (Emsley & Cowtan, 2004). The stereochemical quality of the models was checked using *PROCHECK* (Laskowski *et al.*, 1993). Final refinement statistics for all of the LlSAHase complexes are reported in Table 1. The atomic coordinates and structure factors have been deposited in the Protein Data Bank (PDB) with

accession codes 3ond (LlSAHase–adenosine complex), 3one (LlSAHase–adenine complex) and 3onf (LlSAHase–cordycepin complex).

2.3. Determination of the oligomeric state

To confirm the homodimeric form of LlSAHase, two experiments were carried out. In the first experiment, 2 ml LlSAHase solution (2 mg ml^{-1}) in buffer *A*, consisting of 25 m*M* Tris–HCl pH 8.0, 50 m*M* NaCl, 1 m*M* TCEP, was loaded onto an ultrafiltration membrane with a molecular-weight cutoff of 150 kDa (Pierce Concentrator 7 ml/150K). After a complete cycle of centrifugation (total volume passed through the membrane), the protein concentration in the supernatant was measured. In the second experiment, size-exclusion chromatography was used to separate a mixture of LlSAHase (110 kDa per dimer) and *Thermotoga maritima* SAHase (180 kDa, tetramer). A mixture of the two proteins (1 mg of each) in 1 ml buffer *B*, consisting of 25 m*M* Tris–HCl pH 8.0, 100 m*M* NaCl, 1 m*M* TCEP, was loaded onto a Superdex 200 HiLoad 26/60 column (GE Healthcare) equilibrated with buffer *B*. Fractions corresponding to each enzyme were pooled and analyzed using SDS–PAGE.

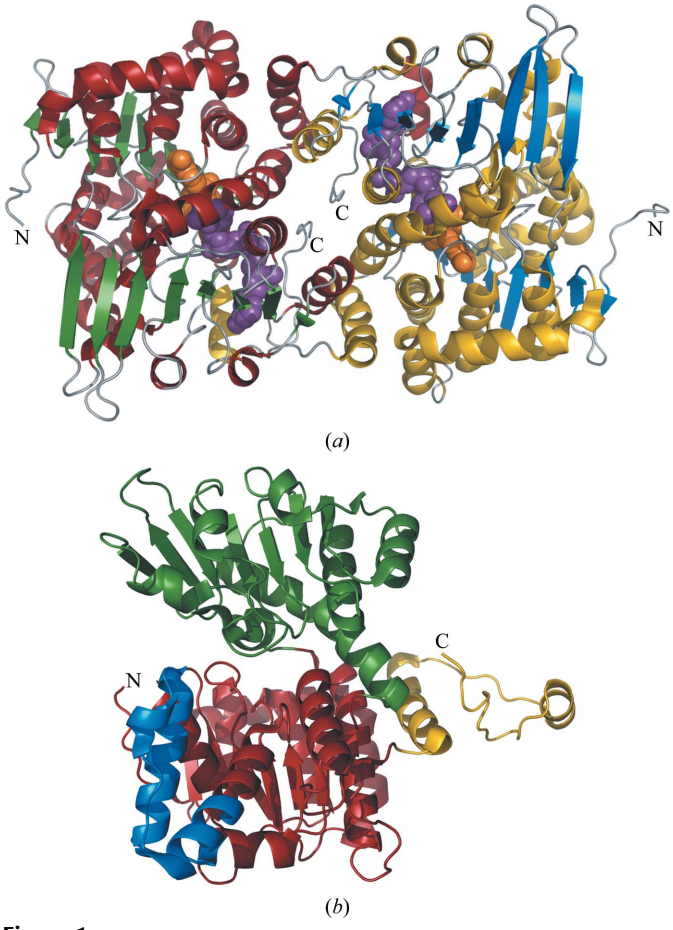

Figure 1
Overall structure of LlSAHase. (*a*) A ribbon diagram of the LlSAHase *AB* homodimer. The NAD$^+$ cofactor (purple) and adenosine (orange) are shown in space-filling representation. β-Strands are shown in green and blue, and α-helices in red and gold, for the *A* and *B* subunits, respectively. (*b*) The structure of one LlSAHase subunit with colour-coded domains: the substrate-binding domain (residues 1–230 and 404–438) is shown in red, the insertion segment located in the substrate-binding domain (residues 151–191) is shown in blue, the cofactor-binding domain (residues 231–403) is shown in green and the C-terminal domain (residues 439–485) is shown in gold.

2.4. Assays of SAHase activity and inhibition

Assays of LlSAHase activity in the hydrolytic direction as well as an inhibition study were carried out spectrophotometrically and the rate of Hcy formation was measured by monitoring its reaction with DTNB [Ellman's reagent; 5,5′-dithio-bis-(2-nitrobenzoic acid); Ellman, 1959; Yuan *et al.*, 1996]. Assays were performed in 200 µl using 0.35 mg LlSAHase (measured spectrophotometrically at 280 nm) and four units of adenosine deaminase in a buffer composed of 100 µ*M* DTNB, 50 m*M* NaCl and 25 m*M* Tris–HCl pH 8.0. The reaction was initiated by addition of SAH to a final concentration of 100 µ*M*. The conversion of Hcy to Hcy-TNB was carried out at 293 K. The progress of the reaction was measured for 1 min and monitored at 412 nm. Initial velocity parameters were estimated from the linear region of the recorded curve. For the inhibition study, SAH was added to the reaction mixture after 5 min of incubation with adenosine or cordycepin, or immediately after the addition of 2′-deoxyadenosine. For each nucleoside, concentrations from 1 to 4000 µ*M* were assayed to determine the IC_{50} constants.

The oxidized:reduced cofactor ratio in samples of purified recombinant LlSAHase as well as the time-dependent inactivation of the enzyme by 2′-deoxyadenosine were monitored spectrofluorometrically by excitation at 340 nm and measurement of emission at 460 nm, as described by Yuan *et al.* (1993). For the inactivation study, the reaction was initiated by the addition of 2′-deoxyadenosine (final concentration of 1 m*M*) to 600 µl reaction mixture consisting of 0.8 mg LlSAHase in a buffer composed of 50 m*M* NaCl and 25 m*M* Tris–HCl pH 8.0. The reaction was carried out at 293 K and was monitored for 80 min until the intensity of fluorescence emission reached a plateau. Analogous experiments were carried out for adenosine and cordycepin with concomitant NAD$^+$:NADH ratio determination.

3. Results and discussion

3.1. Overall structure of plant SAHase

The enzyme crystallizes in space group $P4_32_12$ with two subunits, labelled *A* and *B*, in the asymmetric unit (Fig. 1*a*). The two subunits form the biologically relevant homodimeric enzyme (see §3.6). Each subunit is comprised of 485 amino-acid residues, has a molecular mass of about 55 kDa and contains a tightly but noncovalently bound NAD$^+$ cofactor. Each protomer (Fig. 1*b*) consists of two large domains, the substrate-binding domain and the cofactor-binding domain, separated by a deep cleft. In addition, there is a small C-terminal domain. All three complexes crystallized with the ligand-induced closed conformation.

The substrate-binding domain corresponds to residues 1–230 and 404–438. It has an α/β-type fold as observed in the

previously reported structures. The central mixed β-sheet is formed by nine strands with topology 1, 3x, −1x, −1x, 3x, 1x, 1x, 1x. The cofactor-binding domain, comprised of residues 231–403, adopts an unusual Rossmann fold with variation in the topological connection of the $\beta\alpha\beta\alpha\beta$ core (Turner *et al.*, 1998). Eight β-strands form the central β-sheet with topology 1x, 1x, −3x, −1x, −3x, 1, 1. The C-terminal fragment (residues 439–485) adopts a helix–loop–helix–loop structure and plays the role of a dimerization domain. It extends to the adjacent subunit, where it interacts with the cofactor.

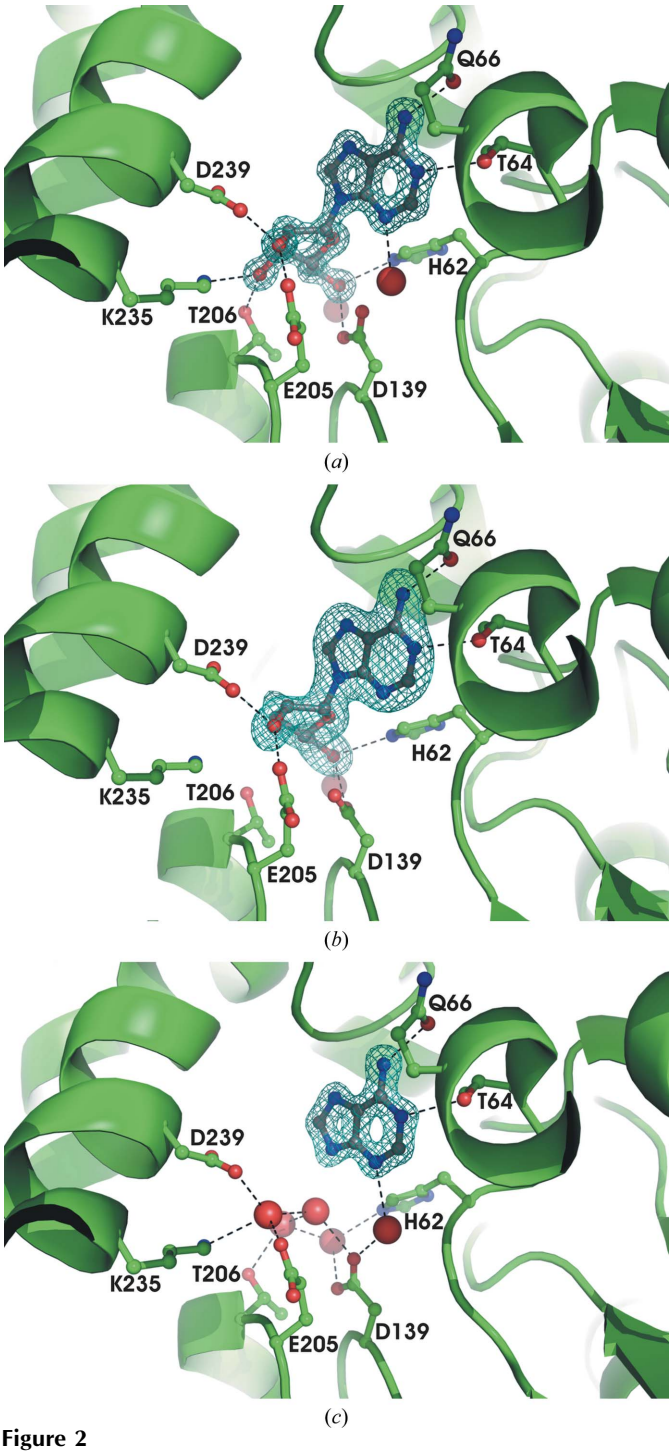

Figure 2
The mode of (*a*) adenosine, (*b*) cordycepin and (*c*) adenine binding in the substrate-binding site of LlSAHase. Only side-chain atoms involved in polar interactions are shown. Possible hydrogen bonds are indicated by broken lines. Water molecules are represented by spheres. The $2F_o - F_c$ electron-density maps are contoured at 2σ for adenosine and adenine and at 1σ for cordycepin.

Table 2
Polar interactions with the ligand molecules bound in the LlSAHase substrate-binding domain, with corresponding donor–acceptor distances (Å) in parentheses.

The interactions in the two subunits are almost identical; therefore, the distances are only listed for chain *A*.

Protein/water atom	Adenosine atom	Cordycepin atom	Adenine atom
Thr64 $O^{\gamma1}$	N1 (2.77)	N1 (2.69)	N1 (2.75)
Wat (*A*)	N3 (2.88)	—	N3 (2.90)
Gln66 $O^{\varepsilon1}$	N6 (2.95)	N6 (3.01)	N6 (2.97)
His404 O	N6 (2.96)	N6 (3.03)	N6 (2.98)
His404 N	N7 (2.92)	N7 (3.02)	N7 (2.86)
Wat (*B*)	—	—	N9 (2.89)
Asp239 $O^{\delta2}$	O2′ (2.51)	O2′ (2.57)	—
Glu205 $O^{\varepsilon2}$	O2′ (2.62)	O2′ (2.73)	—
Lys235 N^{ζ}	O3′ (2.83)	—	—
Thr206 $O^{\gamma1}$	O3′ (2.72)	—	—
Asp139 $O^{\delta1}$	O5′ (2.64)	O5′ (2.68)	—
His62 $N^{\varepsilon2}$	O5′ (2.80)	O5′ (2.90)	—

3.2. Enzyme–ligand interactions

Crystal structures of LlSAHase were determined in complexes with adenosine, cordycepin and adenine. These ligands are found in both subunits and are located in the crevice between the substrate-binding and cofactor-binding domains. Their binding modes are presented in Fig. 2. Polar interactions in the active site for all three ligands are shown in Table 2. Additionally, in all complexes each subunit also contains one nicotinamide adenine dinucleotide molecule. Interactions with all the above ligands are very similar in SAHases of different origin and highly conserved residues are involved in binding the substrate and the cofactor molecules (Fig. 3).

3.2.1. Adenosine. The binding mode of Ado is similar to those observed in eukaryotic and bacterial SAHases complexed with adenosine or its analogs (Turner *et al.*, 1998; Komoto *et al.*, 2000; Tanaka *et al.*, 2004; Reddy *et al.*, 2008). Amino-acid residues from both the substrate-binding and the cofactor-binding domains are involved in Ado binding. The adenine base is anchored in its binding site by several hydrogen bonds. The N6 atom is a donor in two hydrogen bonds, to the carbonyl group of His404 and the side-chain O atom of Gln66, indicating that the purine ring exists in the enolic form. The main-chain N atom of His404 and the side-chain O atom of Thr67 are engaged in interactions with the N7 and N1 atoms, respectively, whereas a water molecule forms a hydrogen bond to N3. Additionally, the side chains of Leu398 and Met409 participate in C—H$\cdots\pi$ and hydrophobic interactions with the purine ring, respectively. The hydroxyl groups of the ribose moiety interact with a water molecule and the imidazole ring of His62 (O5′) and also with the carboxyl groups of Asp139 (O5′), Glu205 and Asp239 (O2′). The side chains of Thr206 and Lys235 form hydrogen bonds to the O3′ atom.

The adenine moiety of Ado is located in a crevice formed by the side-chain atoms of Leu61, Thr64, Gln66, Thr67, Leu398, Met409 and Phe413 and also the main-chain atoms of Leu61, His62 and His404. The latter residue is also involved in sodium coordination. The shape and architecture of the Ado-binding pocket guarantee a perfect fit of the purine ring, as shown in Fig. 4. This result contradicts an earlier study of plant SAHase isolated from tobacco leaves, which suggested that it could serve as a cytokinin-binding protein (Mitsui *et al.*, 1993). Natural cytokinins cannot be bound by LlSAHase, at least not in the adenosine-binding site, owing to steric clashes of the N6 substituent present in these plant hormones. Our results are thus in accord with the observations of Romanov & Deitrich (1995) and Li *et al.* (2008) that plant SAHases do not bind cytokinins and that these phytohormones have no effect on SAHase activity. Along the same lines, N6-modified adenine compounds do not show any inhibitory effects towards human and protozoan SAHases (Tanaka *et al.*, 2004).

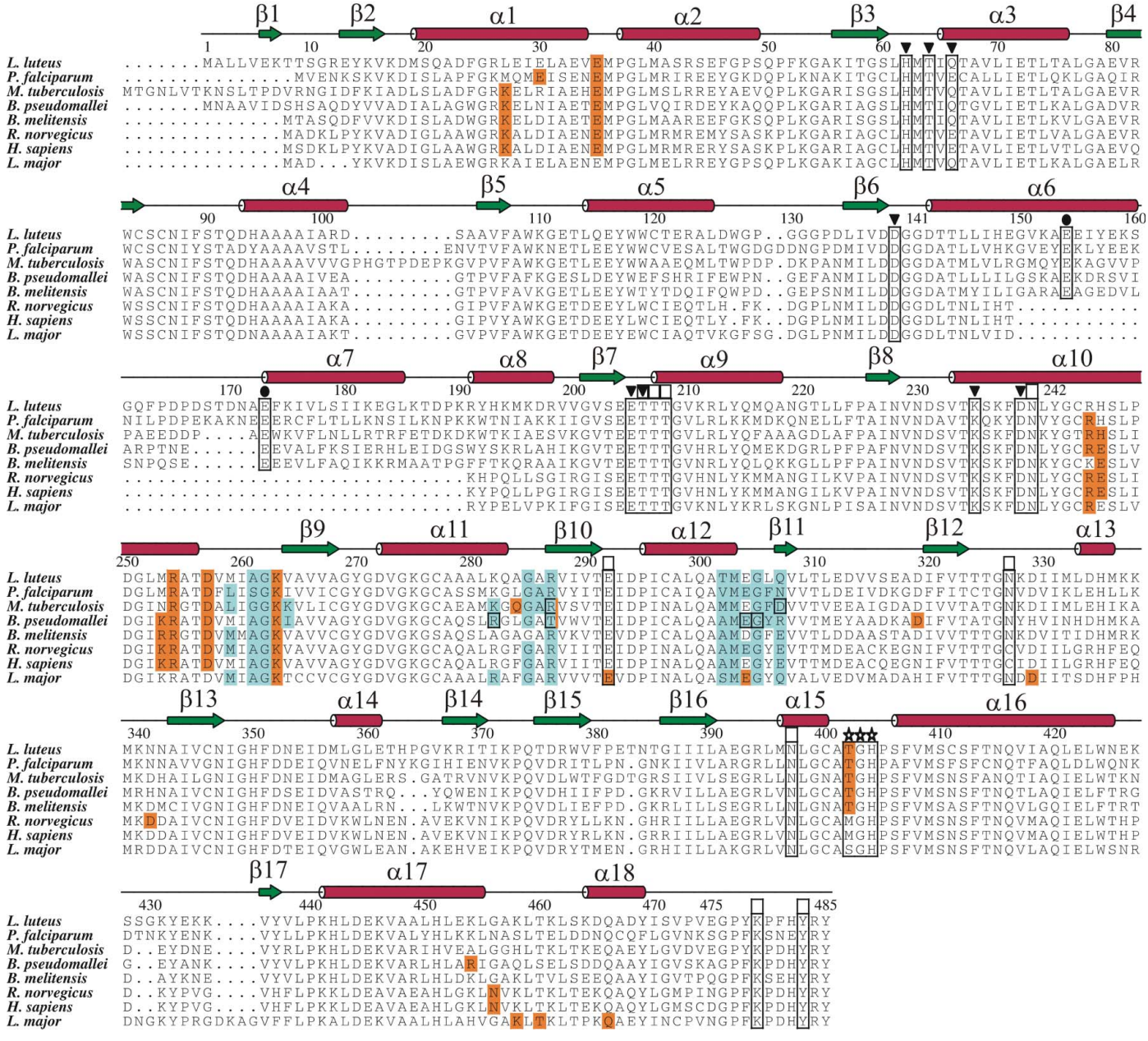

Figure 3
Multiple sequence alignment of selected SAHases. Only structurally characterized homologs of the plant enzyme which are known to be active as tetramers are included. The secondary-structure elements as well as the residue numbers correspond to those of LlSAHase. Residues which interact with ligands are indicated by black triangles (substrate), open squares (cofactor) or stars (Na^+ cation). Black circles correspond to two conserved glutamate residues located in the insertion segment. Residues on a pale-blue background are involved in nonbonded contacts between the *A* and *B*′ subunits within a homotetramer and additionally in hydrogen bonding when boxed. Residues on an orange background participate in similar polar interactions between the *A* and *A*′ subunits. The alignment was calculated in *ClustalW* (Larkin *et al.*, 2007) and the figure was prepared using the *ALINE* editor (Bond & Schüttelkopf, 2009).

3.2.2. Cordycepin. The crystal structure of the LlSAHase–cordycepin complex was determined at a lower resolution (2.0 Å) compared with the other two complex crystals. Despite this, the cordycepin molecule was perfectly defined in the electron-density maps. Its binding mode is similar to that of the enzyme–product complex discussed above. A noticeable difference is the absence of the water molecule engaged in hydrogen bonding to the N3 atom of the ligand. Owing to the absence of the 3′-hydroxyl group, there are no interactions with the Lys235 N^{ζ} and Glu205 $O^{\delta2}$ atoms. As a consequence, the ribose conformation differs from that found in the Ado complex.

3.2.3. Adenine. *S*-Adenosyl-L-homocysteine hydrolase activity is inhibited by 2′-deoxyadenosine (Hershfield, 1979). Enzyme inactivation proceeds *via* the formation of an unstable 3′-keto-2′-deoxyadenosine; the subsequent breakdown of the N-glycosidic bond leads to elimination of the adenine molecule. As a result, NADH (the reduced cofactor) is formed in an irreversible process. Adenine is also a product of glycosidic bond hydrolysis, which is yet another reaction catalyzed by SAHase (Abeles *et al.*, 1980, 1982). The adenine-binding mode is analogous to that observed in the nucleoside complexes described above. The main difference is the absence of the ribose moiety; however, four water molecules mark its place in the active site. Moreover, these water molecules are superposable with the O atoms of the ribose moiety in the adenosine complex within 0.59 Å (O2′), 2.10 Å (O3′), 1.21 Å (O4′) and 0.21 Å (O5′). Thus, the spatial arrangement of the four water molecules mimics the geometry of the hydrophilic groups of a ribofuranose moiety. As a consequence, the residues responsible for interactions with the ribose moiety in the adenosine complex have an identical conformation and form a similar network of hydrogen bonds. None of the amino-acid residues from the cofactor-binding domain are engaged in interactions with the Ade molecule, but the LlSAHase–adenine complex still exists in the closed conformation. This observation supports the proposition that the interactions between the substrate-binding and cofactor-binding domains are strong enough to stabilize the closed conformation of the enzyme (Tanaka *et al.*, 2004).

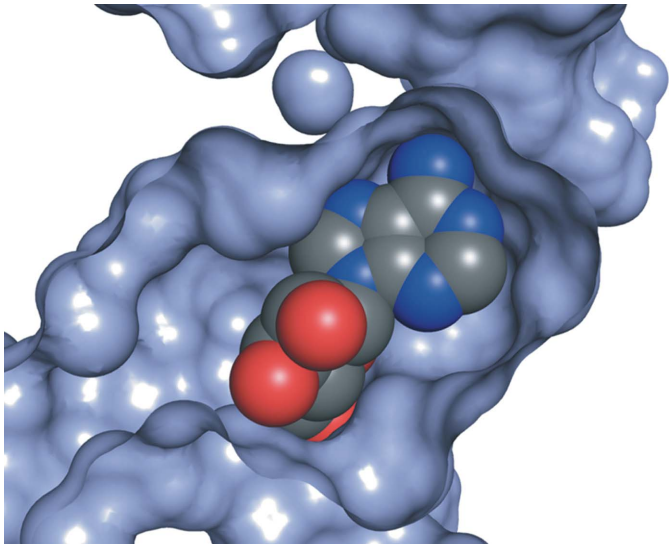

Figure 4
Illustration of the close fit of the adenosine molecule (space-filling model) in the substrate-binding pocket of LlSAHase. The protein is shown in a cutaway surface representation.

Table 3
Conformational analysis of the nucleosides found in the substrate-binding site of LlSAHase.

The interactions in the two subunits are almost identical; therefore, the parameters are only listed for ligands ascribed to chain *A*. The amplitude (τ_m) and phase angle (P) of pseudorotation were calculated according to the method of Jaskólski (1984).

Parameter	Adenosine	Cordycepin
Conformation	*Anti*	*Anti*
Angle (°)		
χ	−105.9 (−*ac*)	−110.7 (−*ac*)
γ	−169.2 (−*ap*)	−175.5 (−*ap*)
ν_0	−39.2	−34.3
ν_1	16.3	6.4
ν_2	11.1	20.5
ν_3	−34.3	−41.2
ν_4	45.0	48.6
τ_m	45.3 (4)	47.7 (9)
P	76.0 (5)	63.6 (10)
Pucker	O4′-*endo* ($^{O}T_4$)	C4′-*exo* ($_4T^{O}$)

3.2.4. Nucleoside conformation. For both nucleosides, the orientation of the nucleobase around the glycosidic bond is *anti* and the position of the O5′ atom relative to the furanose ring, defined by the C3′—C4′—C5′—O5′ torsion angle (γ), is *trans*. The only structural difference between the two nucleosides is the absence of the 3′-hydroxyl group in the cordycepin molecule. This difference between the two ligands has a significant influence on their conformation, especially the phase angle of pseudorotation of the ribose moiety (Table 3). In the case of the enzyme–adenosine complex, the sugar pucker is of O4′-*endo* type ($^{O}T_4$). Such ribose puckering corresponds to a strained conformation that is intermediate between the two principal (C2′-*endo* and C3′-*endo*) modes. This strained conformation of the furan ring is stabilized by two hydrogen bonds between the 3′-hydroxyl group and the Lys235 N^{ζ} and Thr206 $O^{\gamma1}$ atoms. In the cordycepin complex, no stabilization of the sugar conformation through 3′-OH interactions is possible. As a result, the sugar conformation in the LlSAHase–cordycepin complex is less strained: C4′-*exo* ($_4T^{O}$). It is of note that in both cases the puckering amplitude is very high, particularly in cordycepin (47.7°).

3.2.5. Cofactor-binding site. The binding mode of the NAD^+ molecule is very similar to those observed in SAHases from other organisms and the majority of the residues that are involved in cofactor binding are fully conserved. The conformation of the nicotinamide adenine dinucleotide is approximately the same in all three complexes. For the adenine nucleotide part, the orientation around the glycosidic bond is *anti* and the ribose puckering is C1′-*exo*.

The NAD^+ cofactor interacts with the side chains of Asn240, Glu292, Asn327 and Asn397 as well as with main-chain atoms of Asp272, Val273 and Ile348. There are also numerous interactions with the substrate-binding domain,

including the side chains of Thr206, Thr207 and Thr208, which are formed as a result of the conformational change of the enzyme that takes place upon nucleoside binding, in which the substrate-binding domain rotates by about 17–18° towards the NAD^+-binding domain. As in other SAHases, residues from the C-terminal domain of an adjacent subunit within the dimer also participate in cofactor binding. These interactions involve the side chains of the highly conserved Lys479 and Tyr483 that are present in all eukaryotic and bacterial enzymes but not in the archaeal homologs (Stępkowski *et al.*, 2005). Participation of the second subunit in cofactor binding seems to be crucial for enzyme activity. Replacement of Lys426 in human SAHase (which corresponds to Lys479 in LlSAHase) by alanine or glutamate produces inactive mutants which do not bind the cofactor and moreover exist as monomers (Ault-Riché *et al.*, 1994). This observation strongly supports our conclusion (discussed in detail below) that the *AB* dimer of LlSAHase present in the crystallographic asymmetric unit corresponds to the biologically relevant form of the enzyme.

3.3. Ions associated with the LlSAHase molecule

Tris and sodium cations have been identified in all three crystal structures. The presence of Tris ions is a crystallographic artifact. Sodium ions were also present in all purification and crystallization buffers, but their location in the crystal structure strongly indicates their involvement in the enzymatic function. In all three complexes, each protomer binds one sodium cation and the complete coordination sphere has a distorted octahedral geometry provided by three main-chain carbonyl groups (Thr402, Gly403 and His404) and the side chain of Thr402 from a highly conserved loop located between helices α15 and α16 (Fig. 3). In addition, two water molecules complete the coordination sphere of each sodium cation. The interactions of the sodium cation with the enzyme are shown in Fig. 5 and their geometrical details are presented in Table 4. In mammalian SAHases this loop is part of one of two hinge regions involved in substrate-induced domain reorientation (Hu *et al.*, 1999; Turner *et al.*, 2000). In solution, domain oscillations occur in ligand-free enzyme and they are abolished upon ligand binding (Yin *et al.*, 2000). Additionally, mutational studies of the human enzyme indicate that substitution of His353 (equivalent to His404 in the plant enzyme) by alanine slows down the domain movements (Wang *et al.*, 2006). In the plant enzyme, this loop corresponds to residues 401–405. The sodium cation could be speculated to play a role in stabilization of the hinge region during the catalytic cycle. All but one of the SAHase models in the PDB do not have a metal cation in this site. The exception is the bacterial enzyme from *B. melitensis*, which contains potassium ions (present in the crystallization buffer) coordinated at the same site as in LlSAHase. Inspection of the SAHase models deposited in the PDB strongly suggests that this site, usually marked as a 'water' molecule, is indeed occupied by a metal ion coordinated by at least five O atoms. Thus, the elucidation of the biological role of monovalent cations (if any) will require additional studies.

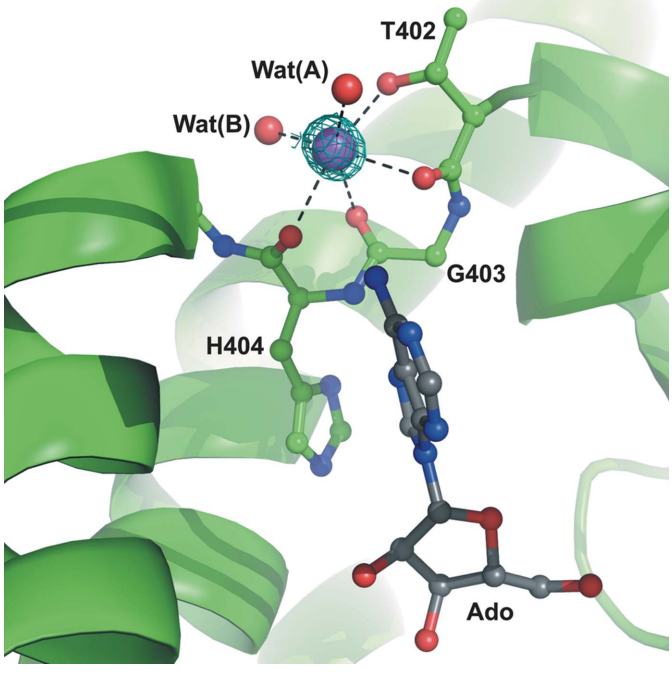

Figure 5
The sodium-coordinating loop located in the proximity of the substrate-binding site of LlSAHase. The Na^+ cation is shown as a purple sphere covered by $2F_o - F_c$ electron-density map contoured at 2σ.

Table 4
Details of sodium coordination in all three complex structures, with the corresponding ligand–Na^+ distances in Å.

The interactions in the two subunits are almost identical; therefore, the distances are only listed only for chain *A*.

Ligand atom	LlSAHase–adenosine	LlSAHase–adenine	LlSAHase–cordycepin
Thr402 $O^{\gamma 1}$	2.50	2.46	2.70
Thr402 O	2.42	2.40	2.54
Gly403 O	2.78	2.65	3.50
His404 O	2.54	2.54	2.80
Wat (*C*)	2.47	2.40	2.36
Wat (*D*)	2.29	2.28	2.63

3.4. Mechanism of SAH hydrolysis

The mechanism of the reversible hydrolysis of *S*-adenosyl-L-homocysteine catalyzed by SAHase was first described by Palmer & Abeles (1979). The first crystal structures of mammalian SAHases directly identified the amino-acid residues involved in the catalytic reaction (Turner *et al.*, 1998; Hu *et al.*, 1999; Komoto *et al.*, 2000; Takata *et al.*, 2002). Since SAHases have rather highly conserved amino-acid sequences and the catalytic residues have remained unchanged during evolution, it is possible to reliably predict the key residues, as well as their function, of the plant enzyme. By analogy to other homologues, we postulate (Fig. 6) that in the initial step of SAH hydrolysis the N^{ζ} atom of Lys235 accepts the proton from the 3′-OH group of the substrate (1). The nucleophilic character of Lys235 is increased by hydrogen bonds to the $O^{\delta 1}$ atoms of Asn230 and Asn240 and to the carbonyl O atom of

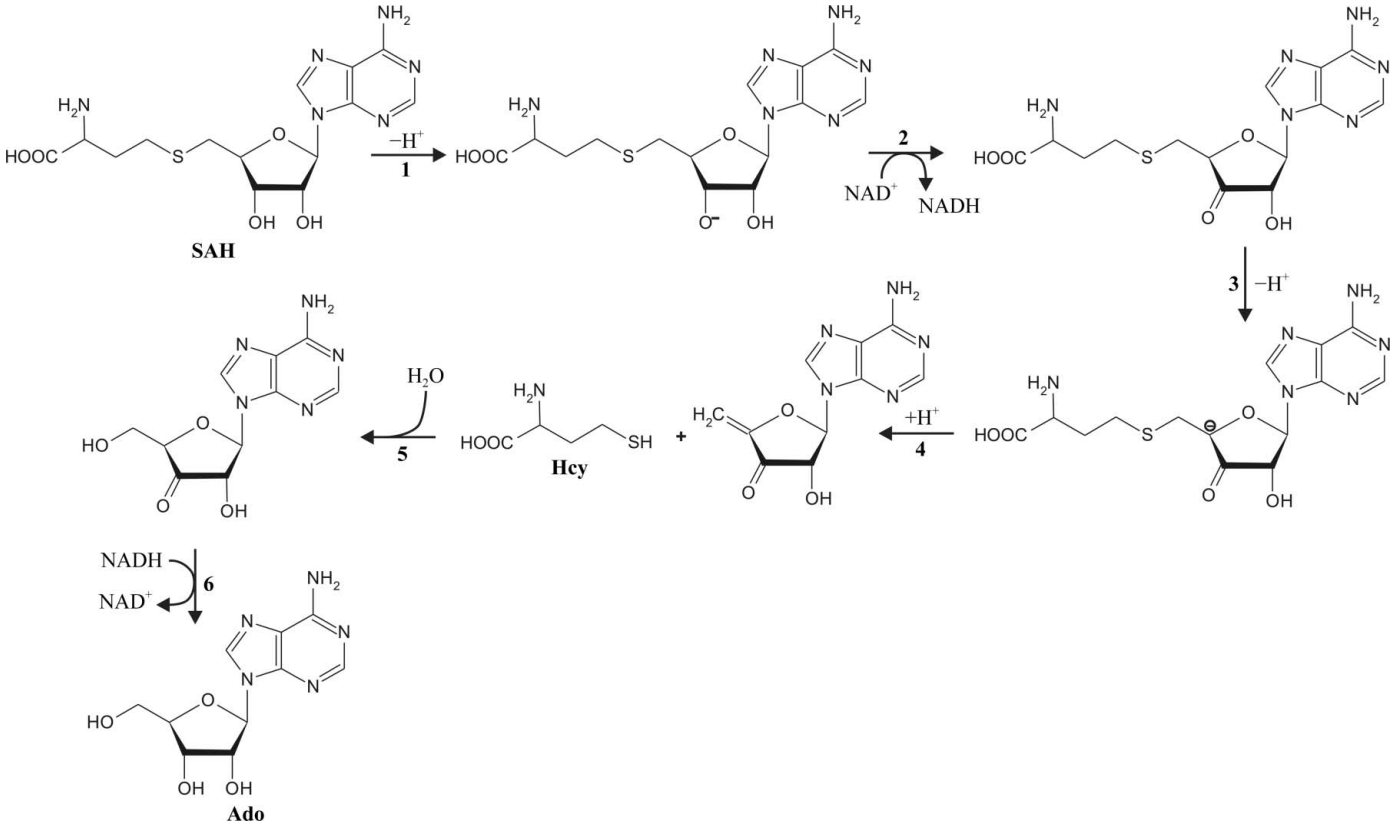

Figure 6
Mechanism of SAH hydrolysis to adenosine (Ado) and L-homocysteine (Hcy) catalyzed by *S*-adenosyl-L-homocysteine hydrolase. The numbers 1–6 indicate the reaction steps described in the mechanism of SAH hydrolysis (see text).

Glu205. As a result, the C3′–H H atom becomes more labile and hydride abstraction by the NAD^+ cofactor is facilitated (2). The products of this reaction step are 3′-keto-AdoHcy and NADH. The acidity of the C4′—H group of the 3′-keto derivative is higher when compared with the Ado molecule, allowing the formation of a $C4'^-$ carboanion through proton transfer to the carboxylic group of Asp139 (3). Proton transfer from the imidazole ring of His62 to the S^{δ} atom of the 3′-keto-AdoHcy carboanion is followed by β-elimination of Hcy, leading to the formation of 3′-keto-4′,5′-didehydroadenosine (4). As the final step, a water molecule is attached through Michael-type addition (5); consequently, the 3′-keto group is reduced and Ado and NAD^+ are generated (6).

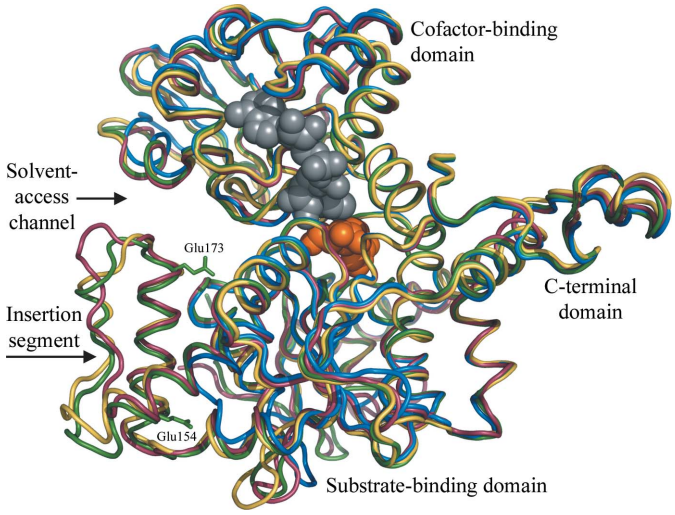

Figure 7
Superposition of the LlSAHase protomer (green) with models of the enzymes from *P. falciparum* (yellow; PDB entry 1v8b), *M. tuberculosis* (raspberry; PDB entry 3ce6) and *H. sapiens* (blue; PDB entry 1li4). The highly conserved Glu154 and Glu173 located in the 40-residue insert of LlSAHase are shown as sticks. Ligands are shown as space-filling models using orange (adenosine) and gray (cofactor) colors.

3.5. The plant-specific insert and the substrate-pocket access channel

An insert of about 40 amino-acid residues is present in all plant SAHases and also in a number of other eukaryotic and bacterial enzymes (Stępkowski *et al.*, 2005). In LlSAHase this segment forms a solvent-exposed region in the catalytic domain (Fig. 7) in an analogous way as in the plasmodial (PDB entry 1v8b) and bacterial (PDB entry 3ce6) enzymes (Tanaka *et al.*, 2004; Reddy *et al.*, 2008). Despite its conserved topology in the protein fold, the insert is in fact the area of the main structural differences between these proteins. The bacterial inserts are several residues shorter, leading to structural divergence. Moreover, differences in the conformation of this surface element could also result from different crystal-packing contacts.

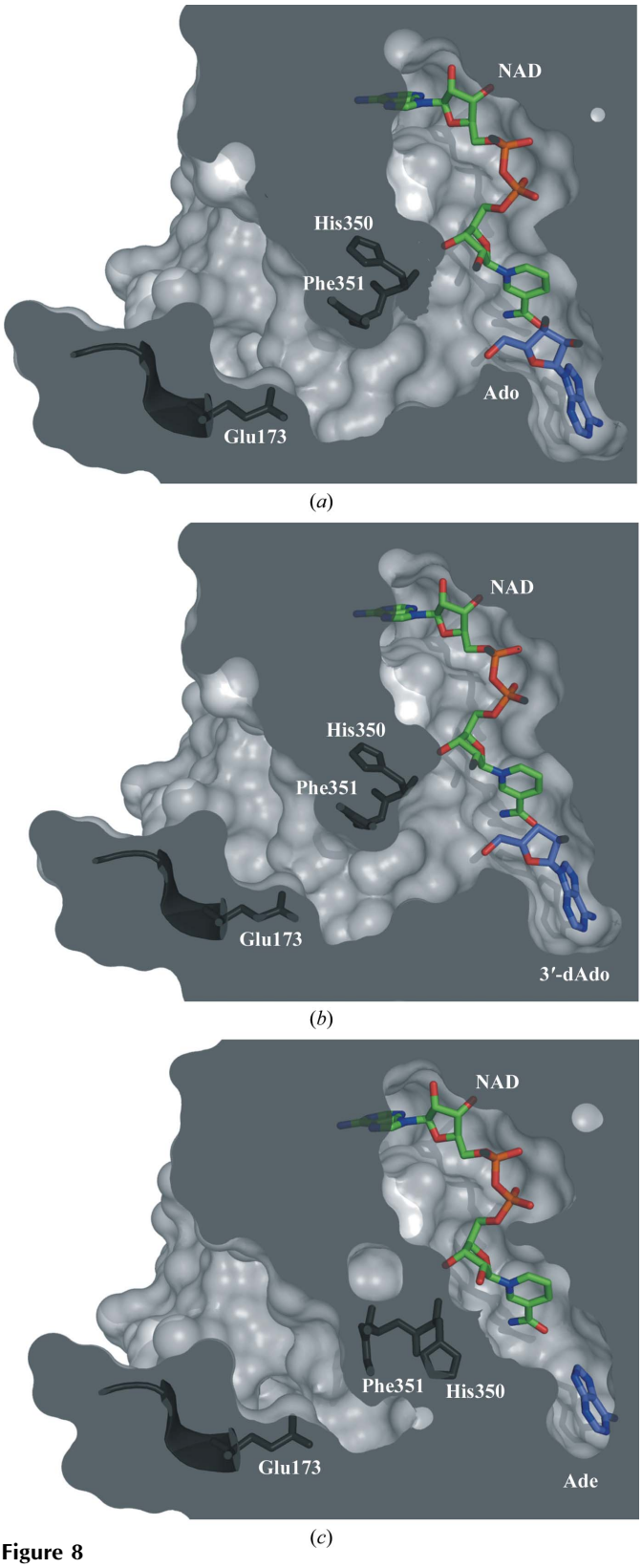

Figure 8
The accessibility of the active site from the solvent region depends on the peptide-plane rotation between residues His350 and Phe351. In the (*a*) adenosine (Ado) and (*b*) cordycepin (3′-dAdo) complexes, the channel is open, whereas in the (*c*) adenine (Ade) complex there is no access to the substrate-binding site. The 40-residue insert forms part of the access channel, as illustrated by the highly conserved Glu173, which is found on its surface.

In yellow lupin SAHase, the insert corresponds to residues 150–190 and adopts a helix–strand–turn–helix structure as observed in other insert-containing enzymes. The first helix of the insert is an extension of an α-helix present in mammalian SAHases (helix α10 in human SAHase annotation). The reasons why plant and most bacterial SAHases possess the additional 40-residue segment, as well as its function, are not well understood. However, it has been pointed out that owing to the absence of the insert in mammalian enzymes, the mouth to the access channel leading to the substrate-binding pocket is more open when compared with insert-possessing SAHases (Reddy *et al.*, 2008). Moreover, part of the insertion region is involved in the formation of the access channel itself. Also, in contrast to the mammalian enzymes, more bulky residues are found to form the walls of the access channel, rendering it more constricted. Similar conclusions are true for the plant enzyme, in which the insert is located near the substrate-binding pocket access channel and constrains the mouth of the channel considerably (Fig. 8). There are two conserved positions found in the insert region. The first one, a highly conserved Glu154, is located far from the channel and the active site and its potential role is unclear. The strictly conserved Glu173 projects into the access channel but lies far from the substrate-binding site. This indicates that it is not directly engaged in the catalytic reaction. However, as part of the channel structure it could participate in substrate/product transfer to/from the active site.

It was observed by Reddy *et al.* (2008) that the solvent channel could be open or closed by the His363 side chain, which functions as a 'molecular gate' through a mechanism based on a 180° flip of the peptide plane between the C^{α} atoms of the conserved histidine and phenylalanine residues. In the plant enzyme, these residues correspond to His350 and Phe351. In all SAHases this peptide flip would lead to significant changes in several torsion angles. When the channel is open, the histidine residue adopts a β-strand conformation, while the next phenylalanine is found in the P-region of the Ramachandran plot. When the channel is closed, the φ/ψ angles of His350 and Phe351 correspond to the α-region and the β-region, respectively.

Access to the active site seems to be regulated differently in SAHase homologues of different origin. In the *M. tuberculosis* SAHase–adenosine complex (PDB entry 3ce6) the channel is closed, whereas it is open in the SAH complex (PDB entry 3dhy) to avoid steric clashes of the imidazole ring of His363 with the homocysteine moiety of the SAH molecule (Reddy *et al.*, 2008). In other bacterial and eukaryotic SAHases the channel is also closed when adenosine or its analogues are bound. Plasmodial and plant enzymes are exceptions in this respect as the channel is open in complexes with adenosine, as illustrated in Fig. 8 for the LlSAHase–adenosine complex. An analogous situation is observed in the LlSAHase–cordycepin complex. The open channel could indicate that the enzyme is ready to transfer the second reagent, *i.e.* a molecule of L-homocysteine, to start the synthesis reaction. The opposite His350—Phe351 peptide-plane orientation is found in the LlSAHase–adenine complex, in which the channel is closed

Table 5
Selected hits found by a *Secondary-Structure Matching* (*SSM*) search with chain *A* from the LlSAHase–adenosine complex as the query, corresponding to different SAHase models in closed conformation.

The *Q*-score represents the quality function of the C^{α} alignment, with the maximum being 1.00 for 100% identical structures; r.m.s.d., C^{α} root-mean-square deviation (Å) between LlSAHase and the target enzyme; N_{align}, number of matched residues or length of alignment; $\%_{seq}$, percentage sequence identity. Values in parentheses are for similar calculations with the tetramer of LlSAHase present in the crystal lattice (chains *A*, *B*, *A*′, *B*′) used as the query.

Source	PDB code	Chain	*Q*-score	R.m.s.d.	N_{align}	$\%_{seq}$
Plasmodium falciparum	1v8b	*B*	0.90	0.78 (1.01)	471 (1865)	58.4
Mycobacterium tuberculosis	3ce6	*D*	0.88	0.71 (0.95)	469 (1856)	61.6
Burkholderia pseudomallei	3glq	*B*	0.86	0.85 (1.01)	457 (1820)	61.9
Brucella melitensis	3n58	*C*	0.86	0.77 (1.28)	453 (1724)	62.9
Trypanosoma brucei	3h9u	*A*	0.80	0.73 (0.81)	422 (845)	66.8
Rattus norvegicus	1k0u	*F*	0.79	0.86 (1.12)	422 (1699)	64.2
Homo sapiens	1li4	*A*	0.78	0.87 (1.03)	421 (1686)	63.4
Leishmania major	3g1u	*C*	0.75	0.81 (1.11)	407 (1607)	65.1

and the adenine molecule is trapped. This explains why adenine cannot be easily removed, even with prolonged dialysis, after 2′-deoxyadenosine cleavage (Abeles *et al.*, 1980).

3.6. LlSAHase *versus* other *S*-adenosyl-L-homocysteine hydrolases

SAHases are highly conserved enzymes and their structural core is closely related among enzymes of different origin. Protomer comparisons show that their C^{α} traces are superposable within 0.9 Å (Table 5).

3.6.1. LlSAHase forms a dimer in solution. In contrast to other SAHases, which are homotetramers, LlSAHase has been reported to form an enzymatically active dimer in solution (Guranowski & Pawełkiewicz, 1977; Brzezinski *et al.*, 2008). We confirmed these predictions using two experiments. In the first experiment, the total amount of loaded LlSAHase passed a membrane with a 150 kDa cutoff upon ultrafiltration. Since the molecular weight of the LlSAHase monomer is 55 kDa, this result is possible with a dimer (110 kDa) but not with a tetramer (220 kDa). The second experiment used a gel-filtration column to separate LlSAHase and an internal molecular-mass marker (tetrameric SAHase from *T. maritima*, with a molecular mass of about 180 kDa), both at a concentration of 1 mg ml^{-1}. The chromatogram (Fig. 9) showed two distinct well separated elution peaks. The first corresponds to TmSAHase with a higher molecular mass and the second to the present plant enzyme.

3.6.2. Geometric analysis of SAHase oligomeric states. In the crystals of the LlSAHase complexes, the crystallographic twofold axis along the *xy* diagonal generates a tetrameric assembly which corresponds to the oligomeric form found for other SAHases. However, the above experiments clearly indicate that LlSAHase exists in the dimeric state in solution and they also contradict the prediction obtained with the *PISA* server (Krissinel & Henrick, 2007), which suggested a tetramer as a possible oligomeric state in solution. The various interfaces between subunits found by *PISA* are presented in Table 6. Although there is a substantial crystal-packing interface between two *AB* dimers related by the crystallographic dyad, it is of note that the interface between the *A* and *B* subunits within the *AB* dimer is nearly 80% larger, primarily because of the swapped C-terminal domains. A previous study (Ault-Riché *et al.*, 1994) demonstrated that mutations in the C-terminal domain affect the enzyme activity and oligomerization. Moreover, all SAHase crystal structures show that the cofactor-binding site is formed with the participation of the C-terminal domain from another subunit. All these observations point to the *AB* dimer (and not *AA*′, *AB*′ or *BB*′) of LlSAHase as the biologically relevant form (Fig. 10*a*).

The *ABA*′*B*′ agglomerate of LlSAHase generated in the crystal lattice has the same general architecture as all other SAHases that are active as homotetramers (Fig. 10*b*). As presented in Table 5, the plant and plasmodial tetramers are very similar. To explain the oligomeric behaviour of the yellow lupin enzyme and other enzymes in solution, the differences between the *A*–*B* and the nonproductive (*A*–*A*′, *A*–*B*′ or *B*–*B*′) interfaces in all tetramers were inspected, as summarized in Fig. 3 and Table 6. There are no drastic differences between the interface areas and numbers of nonbonded contacts within the *AA*′ and *BB*′ units, although as a rule the interfaces in LlSAHase are inferior. However, the number of hydrogen bonds between these subunits is two to three times smaller in the plant enzyme. The *A*–*B*′ interface is highly similar in all enzymes with regards to the intersubunit area and interactions. This suggests that the main determinant of tetramerization is the (higher) number of hydrogen bonds within the *A*–*A*′ and *B*–*B*′ interfaces that is observed in nonplant SAHases but not in LlSAHase.

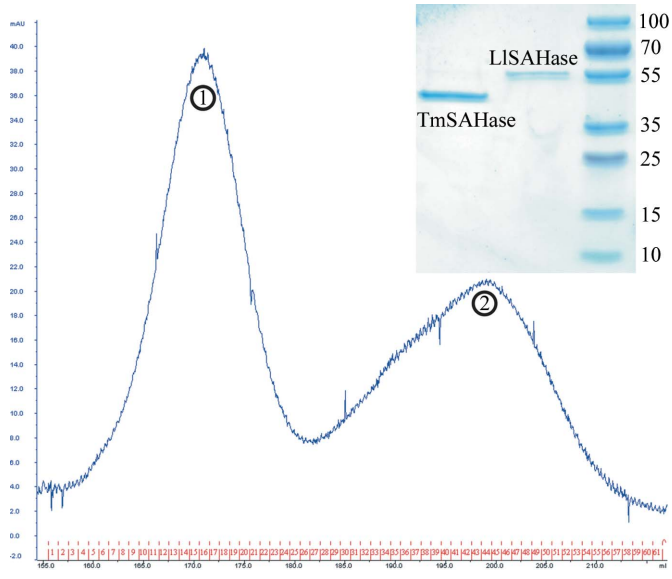

Figure 9
Size-exclusion chromatographic separation of a mixture of TmSAHase (180 kDa as a homotetramer) and LlSAHase (110 kDa as a homodimer) shows two distinct peaks. Peak fractions were loaded on SDS–PAGE to confirm the order of elution: monomer of TmSAHase, 45 kDa (peak 1); monomer of LlSAHase, 55 kDa (peak 2). The molecular masses of the markers (lane 3) are shown in kDa.

Table 6
Results of intradimer interaction-interface searches obtained with the *PISA* server (Krissinel & Henrick, 2007) for the LlSAHase model and its homologues which are known to be active as tetramers.

The following PDB coordinates were used: 3ond (this work), 1v8b (*P. falciparum*), 3ce6 (*M. tuberculosis*), 3glq (*B. pseudomallei*), 3n58 (*B. melitensis*), 1k0u (*R. norvegicus*), 1li4 (*H. sapiens*), 3g1u (*L. major*). In *PISA* calculations for LlSAHase two symmetrically related chains, A' and B', were generated using the crystallographic twofold axis along *xy* to obtain a tetrameric assembly similar to SAHases from other (nonplant) organisms. Chains A' and B' are crystallographic (twofold-symmetric) copies of chains *A* and *B* of LlSAHase and correspond to chains *C* and *D* in the other enzymes, respectively. The interface area is calculated as the difference in the total accessible surface areas of isolated and interfacing structures divided by two. The numbers of contacts across the interfaces were established by *PDBsum* (Laskowski, 2009); N_P is the number of polar interactions across the interface and N_{NBC} is the number of nonbonded contacts across the interface.

Interface type	Enzyme source	Interface area (Å)	N_P	N_{NBC}
A–*B*	*L. luteus*	2911	28	323
	P. falciparum	2860	20	266
	M. tuberculosis	3075	31	328
	B. pseudomallei	2864	29	310
	B. melitensis	2728	20	273
	R. norvegicus	2988	28	388
	H. sapiens	2891	28	324
	L. major	1909	21	177
A–*A*′	*L. luteus*	1651	6	125
	P. falciparum	1939	14	123
	M. tuberculosis	1668	16	151
	B. pseudomallei	1751	22	192
	B. melitensis	1661	16	149
	R. norvegicus	1691	14	158
	H. sapiens	1730	16	158
	L. major	1799	12	156
B–*B*′	*L. luteus*	1618	6	123
	P. falciparum	1921	12	136
	M. tuberculosis	1665	16	148
	B. pseudomallei	1750	22	178
	B. melitensis	1496	13	126
	R. norvegicus	1714	15	163
	H. sapiens	1730	16	158
	L. major	1789	12	156
A–*B*′	*L. luteus*	443	—	49
	P. falciparum	468	—	44
	M. tuberculosis	456	—	55
	B. pseudomallei	488	6	66
	B. melitensis	368	—	31
	R. norvegicus	415	—	38
	H. sapiens	403	—	54
	L. major	446	—	46

The apparently inconsistent results regarding the quaternary structure of LlSAHase can be reconciled if one assumes that the oligomeric state depends on the protein concentration. At lower concentration the enzyme certainly exists as a dimer, while at high nonphysiological concentrations, for example as found during the crystallization process, further oligomerization is possible. Taking into account the fact that all other known SAHases exist as homotetramers, one could speculate that the LlSAHase tetramer in a crystalline state is a kind of evolutionary residual. Additional studies would be required to clarify this phenomenon.

3.7. Enzymatic studies

The following kinetic parameters characterizing the enzymatic activity of recombinant LlSAHase towards SAH hydrolysis have been determined: $K_m = 9.8 \pm 1.2\ \mu M$, $V_{max} = (2.3 \pm 0.02) \times 10^{-7}\ M\ s^{-1}$ and $k_{cat} = 0.022 \pm 0.002\ s^{-1}$. The Michaelis–Menten constant is in good agreement with that for the enzyme isolated from yellow lupin seeds (12 μM) reported by Guranowski & Pawełkiewicz (1977).

Inhibition assays only permitted the calculation of IC_{50} values for adenosine and 2′-deoxyadenosine. The analysis was carried out for a wide range of nucleoside concentrations from 1 to 4000 μM. The IC_{50} value for adenosine is $67 \pm 6\ \mu M$. On the other hand, cordycepin and 2′-deoxyadenosine appear to be very weak competitors. Cordycepin did not significantly affect the SAHase reaction rates even at very high

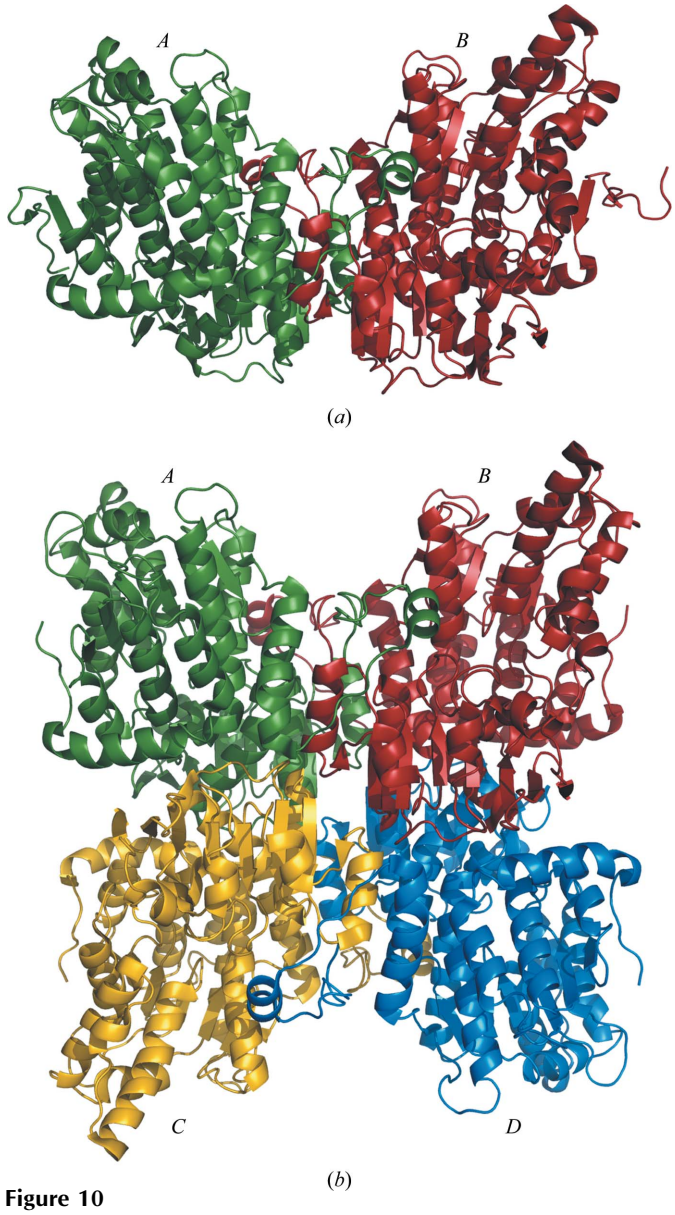

Figure 10
(*a*) *L. luteus S*-adenosyl-L-homocysteine hydrolase (LlSAHase) is active in a homodimeric *AB* form. (*b*) Animal, bacterial and plasmodial SAHases are active as *ABCD* homotetramers; the *P. falciparum* enzyme (PDB entry 1v8b) is shown as an example. In the LlSAHase crystal, subunits A' and B' are generated by the crystallographic twofold axis along the *xy* diagonal and correspond to the *C* and *D* chains, respectively, of the plasmodial enzyme.

concentration (4 m*M*). 2′-Deoxyadenosine inactivates the enzyme by irreversible reduction of the cofactor and by trapping adenine in the active site. For the competition test, the reaction was started immediately without any incubation of the enzyme with this nucleoside in order to minimize the influence of irreversible inactivation. 2′-Deoxyadenosine reduces the enzyme velocity by half at a concentration of about 2.7 m*M*. Such large differences in IC_{50} could indicate that the presence of two hydroxyl groups at the sugar ring favor adenosine as a stronger inhibitor.

Determination of the NAD^+:NADH ratio in purified recombinant LlSAHase indicates that about 95% of the cofactor exists in the oxidized NAD^+ form. Time-dependent inactivation of LlSAHase by 2′-deoxyadenosine showed that the accumulation of NADH increases over 80 min until the emission intensity curve reaches a plateau. After the reaction, the NAD^+ content is ∼10–15% and the rest of the cofactor exists in the reduced NADH form. This suggests that during enzyme inactivation by 2′-deoxyadenosine, the adenine molecule is formed mainly in a redox process in which NAD^+ is irreversibly converted to its reduced form and the enzyme becomes inactive. The second decomposition reaction, hydrolysis of 2′-deoxyadenosine, is insignificant, at least for the plant enzyme. Adenosine and cordycepin did not increase the intensity of fluorescence emission under similar conditions, which confirms that they do not reduce the cofactor.

4. Conclusions

Recombinant SAHase from yellow lupin has been crystallized in the presence of adenosine, of 3′-deoxyadenosine and of 2′-deoxyadenosine. The latter ligand was converted by the active enzyme to adenine (Ade), which was unambiguously detected in the ligand-binding site in excellent-quality electron-density maps. The crystals of the adenosine and adenine complexes diffracted X-rays to atomic resolution. The asymmetric unit of the investigated crystals contains a homodimeric protein corresponding to the active form of this plant SAHase. Although crystallographic symmetry within the crystal generates a tetrameric assembly corresponding to a homotetramer similar to the biologically active form of SAHases from other organisms, our additional experiments demonstrate beyond doubt that the *L. luteus* enzyme exists in a dimeric form in solution at physiological concentrations. However, further oligomerization to form a tetramer is possible at high nonphysiological concentrations or can be forced by crystal packing. In addition to the Ado, Ade or cordycepin ligands found in the substrate-binding domain, each subunit contains a tightly bound NAD^+ molecule in the cofactor-binding domain. In addition to the two principal domains, which are separated by a deep crevice, there is a third small C-terminal domain which plays a role in dimerization.

This work was supported in part by a grant from the Polish Ministry of Science and Higher Education (No. N N302 4305 34), by the Intramural Research Program of NIH, National Cancer Institute, Center for Cancer Research and by Federal funds from the National Cancer Institute, National Institutes of Health under contract HHSN2612008000001E. The content of this publication does not necessarily reflect the views or policies of the Department of Health and Human Services, nor does the mention of trade names, commercial products, or organizations imply endorsement by the US Government.

References

Abeles, R. H., Fish, S. & Lapinskas, B. (1982). *Biochemistry*, **21**, 5557–5562.
Abeles, R. H., Tashjian, A. H. & Fish, S. (1980). *Biochem. Biophys. Res. Commun.* **95**, 612–617.
Alawady, A. E. & Grimm, B. (2005). *Plant J.* **41**, 282–290.
Ault-Riché, D. B., Yuan, C.-S. & Borchardt, R. T. (1994). *J. Biol. Chem.* **269**, 31472–31478.
Bond, C. S. & Schüttelkopf, A. W. (2009). *Acta Cryst.* D**65**, 510–512.
Brzezinski, K., Bujacz, G. & Jaskolski, M. (2008). *Acta Cryst.* F**64**, 671–673.
Brzeziński, K., Janowski, R., Podkowiński, J. & Jaskólski, M. (2001). *Acta Biochim. Pol.* **48**, 477–483.
Chiang, P. K. (1998). *Pharmacol. Ther.* **77**, 115–134.
Chiang, P. K. & Cantoni, G. L. (1979). *Biochem. Pharmacol.* **28**, 1897–1902.
De La Haba, G. & Cantoni, G. L. (1959). *J. Biol. Chem.* **234**, 603–608.
Ellman, G. L. (1959). *Arch. Biochem. Biophys.* **82**, 70–77.
Elmayan, T., Balzergue, S., Béon, F., Bourdon, V., Daubremet, J., Guénet, Y., Mourrain, P., Palauqui, J. C., Vernhettes, S., Vialle, T., Wostrikoff, K. & Vaucheret, H. (1998). *Plant Cell*, **10**, 1747–1758.
Emsley, P. & Cowtan, K. (2004). *Acta Cryst.* D**60**, 2126–2132.
Fulneček, J., Matyášek, R., Votruba, I., Holý, A., Křížová, K. & Kovařík, A. (2011). *Mol. Genet. Genomics*, **285**, 225–236.
Guranowski, A. & Pawełkiewicz, J. (1977). *Eur. J. Biochem.* **80**, 517–523.
Hershfield, M. S. (1979). *J. Biol. Chem.* **254**, 22–25.
Housen, I., Demonté, D., Lafontaine, D. & Vandenhaute, J. (1997). *Yeast*, **13**, 777–781.
Hu, Y., Komoto, J., Huang, Y., Gomi, T., Ogawa, H., Takata, Y., Fujioka, M. & Takusagawa, F. (1999). *Biochemistry*, **38**, 8323–8333.
Huang, Y., Komoto, J., Takata, Y., Powell, D. R., Gomi, T., Ogawa, H., Fujioka, M. & Takusagawa, F. (2002). *J. Biol. Chem.* **277**, 7477–7482.
Jaskólski, M. (1984). *Acta Cryst.* A**40**, 364–366.
Jones, L., Ratcliff, F. & Baulcombe, D. C. (2001). *Curr. Biol.* **11**, 747–757.
Kinoshita, T., Miura, A., Choi, Y., Kinoshita, Y., Cao, X., Jacobsen, S. E., Fischer, R. L. & Kakutani, T. (2004). *Science*, **303**, 521–523.
Komoto, J., Huang, Y., Gomi, T., Ogawa, H., Takata, Y., Fujioka, M. & Takusagawa, F. (2000). *J. Biol. Chem.* **275**, 32147–32156.
Krissinel, E. & Henrick, K. (2007). *J. Mol. Biol.* **372**, 774–797.
Lafontaine, D., Delcour, J., Glasser, A. L., Desgrès, J. & Vandenhaute, J. (1994). *J. Mol. Biol.* **241**, 492–497.
Larkin, M. A., Blackshields, G., Brown, N. P., Chenna, R., McGettigan, P. A., McWilliam, H., Valentin, F., Wallace, I. M., Wilm, A., Lopez, R., Thompson, J. D., Gibson, T. J. & Higgins, D. G. (2007). *Bioinformatics*, **23**, 2947–2948.
Laskowski, R. A. (2009). *Nucleic Acids Res.* **37**, D355–D359.
Laskowski, R. A., MacArthur, M. W., Moss, D. S. & Thornton, J. M. (1993). *J. Appl. Cryst.* **26**, 283–291.
Li, C.-H., Yu, N., Jiang, S.-M., Shangguan, X.-X., Wang, L.-J. & Chen, X.-Y. (2008). *Planta*, **228**, 125–136.
McCoy, A. J., Grosse-Kunstleve, R. W., Adams, P. D., Winn, M. D., Storoni, L. C. & Read, R. J. (2007). *J. Appl. Cryst.* **40**, 658–674.

Migchielsen, A. A., Breuer, M. L., van Roon, M. A., te Riele, H., Zurcher, C., Ossendorp, F., Toutain, S., Hershfield, M. S., Berns, A. & Valerio, D. (1995). *Nature Genet.* **10**, 279–287.
Mitsui, S., Wakasugi, T. & Sugiura, M. (1993). *Plant Cell Physiol.* **34**, 1089–1096.
Moffatt, B. A., Stevens, Y. Y., Allen, M. S., Snider, J. D., Pereira, L. A., Todorova, M. I., Summers, P. S., Weretilnyk, E. A., Martin-McCaffrey, L. & Wagner, C. (2002). *Plant Physiol.* **128**, 812–821.
Morel, J. B., Mourrain, P., Béclin, C. & Vaucheret, H. (2000). *Curr. Biol.* **10**, 1591–1594.
Mull, L., Ebbs, M. L. & Bender, J. (2006). *Genetics*, **174**, 1161–1171.
Müller, P., Köpke, S. & Sheldrick, G. M. (2003). *Acta Cryst.* D**59**, 32–37.
Murshudov, G. N., Skubák, P., Lebedev, A. A., Pannu, N. S., Steiner, R. A., Nicholls, R. A., Winn, M. D., Long, F. & Vagin, A. A. (2011). *Acta Cryst.* D**67**, 355–367.
Ofengand, J. (2002). *FEBS Lett.* **514**, 17–25.
Otwinowski, Z. & Minor, W. (1997). *Methods Enzymol.* **276**, 307–326.
Palmer, J. L. & Abeles, R. H. (1979). *J. Biol. Chem.* **254**, 1217–1226.
Pereira, L. A., Todorova, M., Cai, X., Makaroff, C. A., Emery, R. J. & Moffatt, B. A. (2007). *J. Exp. Bot.* **58**, 1083–1098.
Poulton, J. E. & Butt, V. S. (1975). *Biochim. Biophys. Acta*, **403**, 301–314.
Poulton, J. E. & Butt, V. S. (1976). *Arch. Biochem. Biophys.* **172**, 135–142.
Reddy, M. C., Kuppan, G., Shetty, N. D., Owen, J. L., Ioerger, T. R. & Sacchettini, J. C. (2008). *Protein Sci.* **17**, 2134–2144.
Richards, H. H., Chiang, P. K. & Cantoni, G. L. (1978). *J. Biol. Chem.* **253**, 4476–4480.
Rocha, P. S., Sheikh, M., Melchiorre, R., Fagard, M., Boutet, S., Loach, R., Moffatt, B., Wagner, C., Vaucheret, H. & Furner, I. (2005). *Plant Cell*, **17**, 404–417.
Romanov, G. A. & Deitrich, A. (1995). *Plant Sci.* **107**, 77–81.
Seidel-Rogol, B. L., McCulloch, V. & Shadel, G. S. (2003). *Nature Genet.* **33**, 23–24.
Stępkowski, T., Brzeziński, K., Legocki, A. B., Jaskólski, M. & Béna, G. (2005). *Mol. Phylogenet. Evol.* **34**, 15–28.
Takata, Y., Yamada, T., Huang, Y., Komoto, J., Gomi, T., Ogawa, H., Fujioka, M. & Takusagawa, F. (2002). *J. Biol. Chem.* **277**, 22670–22676.
Tanaka, N., Nakanishi, M., Kusakabe, Y., Shiraiwa, K., Yabe, S., Ito, Y., Kitade, Y. & Nakamura, K. T. (2004). *J. Mol. Biol.* **343**, 1007–1017.
Turner, M. A., Yang, X., Yin, D., Kuczera, K., Borchardt, R. T. & Howell, P. L. (2000). *Cell Biochem. Biophys.* **33**, 101–125.
Turner, M. A., Yuan, C.-S., Borchardt, R. T., Hershfield, M. S., Smith, G. D. & Howell, P. L. (1998). *Nature Struct. Biol.* **5**, 369–376.
Van Buul, C. P., Damm, J. B. & Van Knippenberg, P. H. (1983). *Mol. Gen. Genet.* **189**, 475–478.
Wang, M., Unruh, J. R., Johnson, C. K., Kuczera, K., Schowen, R. L. & Borchardt, R. T. (2006). *Biochemistry*, **45**, 7778–7786.
Winn, M. D., Isupov, M. N. & Murshudov, G. N. (2001). *Acta Cryst.* D**57**, 122–133.
Yang, X., Hu, Y., Yin, D. H., Turner, M. A., Wang, M., Borchardt, R. T., Howell, P. L., Kuczera, K. & Schowen, R. L. (2003). *Biochemistry*, **42**, 1900–1909.
Yin, D., Yang, X., Hu, Y., Kuczera, K., Schowen, R. L., Borchardt, R. T. & Squier, T. C. (2000). *Biochemistry*, **39**, 9811–9818.
Yuan, C.-S., Ault-Riché, D. B. & Borchardt, R. T. (1996). *J. Biol. Chem.* **271**, 28009–28016.
Yuan, C.-S., Yeh, J., Liu, S. & Borchardt, R. T. (1993). *J. Biol. Chem.* **268**, 17030–17037.
Zhang, X., Yazaki, J., Sundaresan, A., Cokus, S., Chan, S. W.-L., Chen, H., Henderson, I. R., Shinn, P., Pellegrini, M., Jacobsen, S. E. & Ecker, J. R. (2006). *Cell*, **126**, 1189–1201.